

Proton production cross sections for reactions by 300- and 392-MeV protons on carbon, aluminum, and niobium

Tadahiro Kin, Fuminobu Saiho, Shinya Hohara, Katsuhiko Ikeda, Kiyohisa Ichikawa, Yusuke Yamashita, Minoru Imamura, Genichiro Wakabayashi, Nobuo Ikeda, Yusuke Uozumi,* and Masaru Matoba
Department of Applied Quantum Physics and Nuclear Engineering, Kyushu University, Fukuoka 812-8581, Japan

Masahiro Nakano
University of Occupational and Environmental Health, Kita-kyushu 807-8555, Japan

Norihiko Koori
Faculty of integrated Arts and Sciences, University of Tokushima, Tokushima 770-8502, Japan
 (Received 22 March 2004; revised manuscript received 24 September 2004; published 14 July 2005;
 publisher error corrected 12 December 2005)

Proton productions from proton induced reactions have been investigated for target nuclei of ^{12}C , ^{27}Al , and ^{93}Nb at 300 and 392 MeV. Proton inelastic continua over a broad energy range were measured at laboratory angles from 20° to 105° . The differential cross sections were compared with two theoretical models, the quantum molecular dynamics (QMD) and the intranuclear cascade (INC) model in terms of the multistep direct process. We demonstrated that consistencies of these models can be improved using a realistic ground state of target nucleus, and that the INC model developed presently has a fairly good consistency and a higher predictive ability than the QMD.

DOI: [10.1103/PhysRevC.72.014606](https://doi.org/10.1103/PhysRevC.72.014606)

PACS number(s): 25.40.Ep, 25.40.Sc, 24.30.Cz

I. INTRODUCTION

Intermediate-energy nuclear data are of high importance in variety of sciences and technologies. Understanding of secondary particle behaviors is necessary to a feasibility study and optimum design of the system offering high safety and low cost.

Proton production cross sections are, in particular, indispensable for estimating the radiation heating and the radiation damage in accelerator-driven systems (ADS) and the radiation dose evaluation in spacecrafts. Energetic protons, as well as neutrons, have received considerable attention because of their fundamental importance in particulate radiation transport models.

To meet the requirement on nuclear data, cross section measurements need to be carried out with covering wide ranges of angular and energy distributions of emitted particles. Although a number of experiments were carried out for cross sections of $(p, p'x)$ reactions in the past, most data were measured at incident energies below 100 MeV and superficial studies have been made at above 200 MeV. It is, therefore, important to investigate $(p, p'x)$ cross sections in the higher energy range above 200 MeV in a systematic way. These experimental data offer also the opportunity to establish the reliability of theoretical calculations, and will contribute to the compilation of high quality nuclear data libraries.

In the present study, energy-angle double differential cross sections of proton productions are investigated for proton incidence upon ^{12}C , ^{27}Al , and ^{93}Nb . Carbon was chosen as one of the targets because the element is a constituent of human body and of importance for the radiation dose evaluation in

spacecrafts. Aluminum and niobium were chosen because they are materials widely used for spacecrafts and ADS.

The incident proton beam energy was chosen to be 300 and 392 MeV. In this energy range, only a few data [1–3] have been reported and no systematic studies were conducted. At around 400 MeV, the real part of nuclear optical potential is known to be very small, and the NN cross sections take their minimum. These facts suggest that the incident proton travels almost straightly and reaches the deep inside of the target nucleus. Then, the target will be brought to a highly excited state via sequent NN collisions, i.e., the multistep direct process. Furthermore, the reaction process can be described within the nucleon degrees of freedom, since pion productions are still negligible. It is, therefore, expected that the data are useful to investigate the multistep process and to improve the accuracy of theoretical models.

From the above point of view, the data obtained presently are compared with theoretical models. In the present work, we examine two semiclassical models: the quantum molecular dynamics (QMD) [4,5] and the intranuclear cascade (INC) [6–15] models, which are widely used for cross section calculations in nuclear data evaluations in an intermediate energy range. Results of these model calculations are considered to be sensitive to distributions of density and momentum in the target nucleus. In terms of the distributions, the predictive abilities of these models are discussed.

In the next section, experimental procedures and apparatus are presented. The method of off-line analyses is explained in Sec. III. In Sec. IV, a brief description of the QMD and the INC used here is given. In addition, we explain a procedure to generate better ground state distributions in the QMD. In Sec. V, results and discussion are described. Our conclusions are presented in Sec. VI.

*Electronic address: uozumi@nucl.kyushu-u.ac.jp

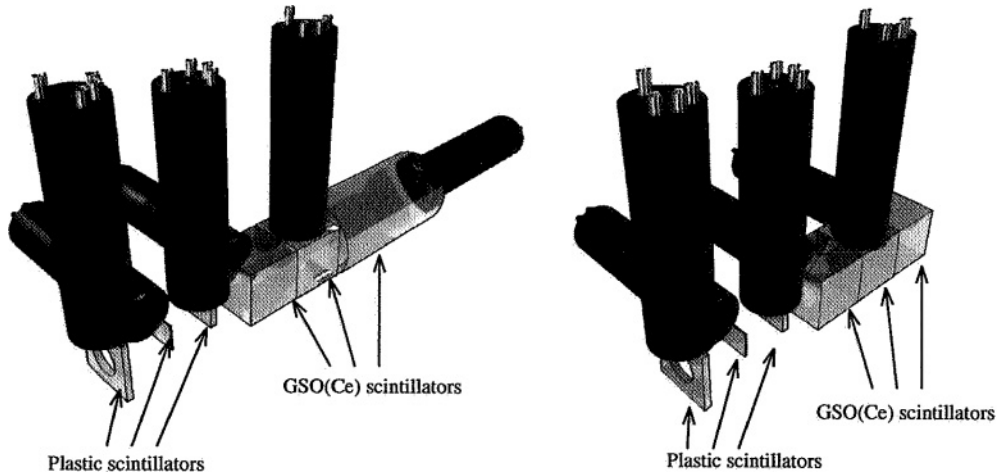


FIG. 1. Stacked GSO(Ce) spectrometers. The long one (left) and the short one (right).

II. EXPERIMENTAL DETAILS

The experiments were conducted at the Research Center for Nuclear Physics, Osaka University. Proton beams were accelerated by the ring cyclotron up to 300 and 392 MeV, and bombarded a target in a vacuum chamber of 800-mm outer diameter. The beam spot was smaller than 5 mm in diameter and centered on the target within 0.5 mm. The integrated beam current was measured during each run in order to determine absolute cross sections. We used a Faraday cup current integrator assembly combined with a CAMAC scaler system, which is believed to be accurate to within 5%. During the experiment, the beam current was in a range of 5 to 10 nA on target. Counting rate was kept low in order to reduce the signal pile-up.

Target foils were mounted on a ladder, which was located at the center of the chamber. Targets used in this experiment were ^{12}C , ^{27}Al , and ^{93}Nb with thickness of 33, 2.7, and 43 mg/cm^2 , respectively. The thickness of these films was determined by weighting with a microbalance and alpha-ray energy loss measurements within uncertainties of $\pm 10\%$. Particles emitted from nuclear reactions were detected by stacked scintillators spectrometers [16,17] placed out of the chamber after flight through a window of the 0.1-mm thick alamid film manufactured by Asahi Chemical Industry Co. and about 110-mm thick air.

The spectrometers were ΔE - E counter telescopes consisting of three plastic scintillators and three GSO(Ce) crystals with modest energy resolution and broad energy acceptance ranging from 40 to 400 MeV. As shown in Fig. 1, we used two types of spectrometers. The long one, which is the left in Fig. 1 consisted of two cubic and a cylindrical GSO(Ce) crystals. The cubic crystals had 43-mm edge lengths. The cylindrical one was 60 mm in diameter and 120 mm in length. The total GSO(Ce) depth was 206 mm, which is enough to stop protons of 400 MeV. Another spectrometer was the short one consisting of three cubic GSO(Ce) crystals and its total GSO(Ce) depth was 129 mm. Each GSO(Ce) crystal of the spectrometers was viewed by a photomultiplier tube. Three plastic scintillators were placed in front of the GSO

crystals of each spectrometer. The first plastic scintillator was a plate of 5 mm thick and 50 mm \times 50 mm square with a circular aperture of 15 mm in diameter at the center. It was used as an active slit. The aperture defined the solid angle of 0.84 mSr subtended by each spectrometer. The second and the third plastic scintillators were plates of 1 and 2 mm thick, respectively, and served as ΔE detectors. A photomultiplier tube viewed one facet of each plastic scintillator through a light guide. The other five facets were covered with aluminum tape for optical isolation. In addition to these, two plastic scintillator detectors were used as a partner detector for the spectrometers during the proton-proton coincidence measurements. These plastic scintillators were plates having a 50 mm \times 50 mm cross section with 5 mm thick and viewed by a photomultiplier tube.

The spectrometers were mounted on a goniometer, which surrounded the chamber; two spectrometers were positioned on opposite sides with respect to the beam in the same reaction plane. The goniometer allowed measurements of angular distributions ranging from 20° to 105° in the laboratory system. The long spectrometer was placed in the forward region mainly. The short one positioned at 105° where high-energy protons appear scarcely during the runs of angular distribution measurements with the long detector.

The signals from the detectors were processed in a standard electronic setup of NIM modules, such as discriminators and coincidence circuitry. The output charges of PMT's were digitized with CAMAC ADC's, and digital data were recorded event-by-event on a hard disk of a PC for subsequent off-line analyses. The coincidence signal of the ΔE plastic scintillators was used to gate open the CAMAC ADC's. The computer dead time was determined for each run by recording the number of coincidence gating pulses in a CAMAC scaler and comparing this with the total number of events analyzed in the computer. Since the counting rate was kept low in order to reduce the signal pile-up, the dead time was less than 10%.

Background due to beam halo, which could distort energy distributions, was measured several times using an empty target frame. Background events were found to be protons of energies lower than 50 MeV. Their contribution to the double differential cross sections is about 1% at 40 MeV of outgoing

energy, and negligible at the higher energies. Then, we made no corrections for distortion due to background.

In advance to the $(p, p'x)$ measurement, elastic proton-proton scattering experiments were carried out using a CH_2 foil target. Angles of spectrometers were changed from 20° to 60° in 10° steps. The partner detector was positioned at the angle determined kinematically according to the angle of each spectrometer. Due to the kinematical coincidence, interference from reaction products from carbon was minimized to a few percent. The $(p, p'x)$ measurement was made to check the following terms. First, the uncertainty of angles was examined by comparing cross sections measured by two spectrometers located symmetrically with respect to the beam. Differences between two spectrometers were negligibly small. And the angular offset of the beam was concluded to be better than 0.5° . Secondly, precision of the absolute cross sections was investigated. Differences from parametrized values [11] were within 10%. The overall systematic uncertainty of absolute cross section values is estimated to be less than $\pm 10\%$ in the present work. Thirdly, energy calibrations of each scintillator were made. In addition to the calibration, energy resolutions were measured. The result is, for instance, 3.2% FWHM for 274-MeV protons.

III. OFF-LINE ANALYSIS

Double differential cross sections were determined through off-line analyses. Pulse heights of signals were converted into particle energy using the light output nonlinearity [17] took into account. Then, the particle identification was carried out by using the parameter PI [18]:

$$PI = E_{\text{total}}^b - (E_{\text{total}} - \Delta E)^b, \quad (1)$$

where b is the parameter representing the range of each particle, E_{total} the total energy deposited on the spectrometer, and the ΔE the amount of energy deposited on the transmission detector.

In Fig. 2 is given a typical two-dimensional plot of PI versus particle energy for the 392-MeV proton induced reaction on ^{93}Nb at 20° . A value of 1.73 was employed for the parameter b , and the ΔE the sum of deposit energies for the two thin plastic scintillators. The thick belt lying at around $PI = 250$ corresponds to proton good events, which stopped in the crystal through the electronic interaction. The lower area is a group of proton bad events, which accidentally underwent nuclear reactions with crystal elements or out-scattering from the crystal volume. Deuteron events distribute in the large PI area. The lines are drawn roughly to guide eyes.

In the present work, double differential cross sections were obtained by the following way. First, PI projection spectra were generated for each energy bin of a 10-MeV width. Next, for each of the spectra, the true events were separated from the false and the deuteron events in terms of PI , and then counted up. The number of proton events was corrected in terms of the peak efficiency that represents the good-to-total ratio. The peak efficiency for the spectrometers had been determined as a function of proton energy with both experiments and Monte Carlo calculations [17]. Finally, the

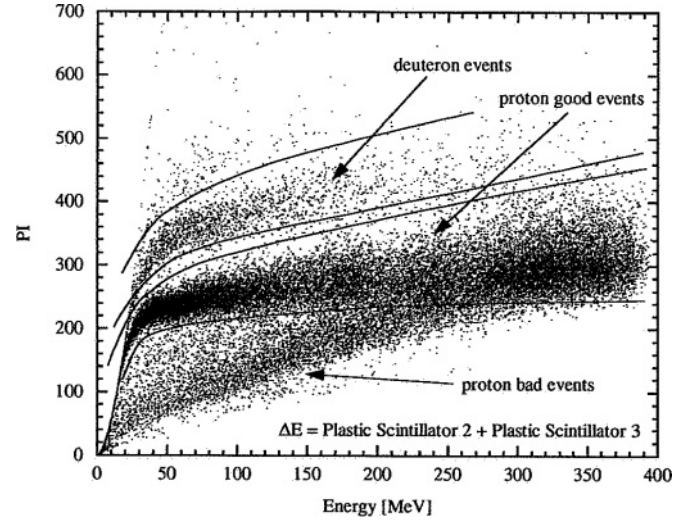


FIG. 2. Plot of PI versus proton kinetic energy obtained for the 392-MeV $^{93}\text{Nb}(p, p'x)$ reaction at 20° . The lines are drawn roughly to guide eyes.

double differential cross sections were determined for each energy bin through a correction for the dead time of the CAMAC-PC data acquisition system.

IV. THEORETICAL MODELS

A. Quantum molecular dynamics model

The QMD model is a semiclassical simulation method, in which a Gaussian wave packet is used to express nucleon states. The time evolution of each nucleon is traced in event-by-event simulations through Newtonian equations of motion in the self-consistent mean field. In the present work, we used the JQMD code. Since the details of the JQMD have been described in Ref. [5], here is given a brief description.

The Hamiltonian H used in the JQMD is defined by

$$H = \sum_i E_i + \frac{1}{2} \frac{C_A}{\rho_0} \sum_i \langle \rho_i \rangle + \frac{1}{1 + \tau} \frac{C_B}{\rho_0^\tau} \times \sum_i \langle \rho_i \rangle^\tau + \frac{C_s}{2\rho_0} \sum_{i,j(\neq i)} (1 - 2|c_i - c_j|) \rho_{ij} + \frac{1}{2} \sum_{i,j(\neq i)} c_i c_j \frac{e^2}{|\mathbf{R}_i - \mathbf{R}_j|} \text{erf} \left(\frac{|\mathbf{R}_i - \mathbf{R}_j|}{\sqrt{4L}} \right). \quad (2)$$

In the right-hand side, the first term E_i is the single particle energy of the i th nucleon. The second and third terms are the Skyrme type potential energy the fourth term the symmetry energy, and the fifth term the Coulomb energy.

In the Skyrme type potential, ρ_0 is the saturation density of 0.168 fm^{-3} . Parameters C_A , C_B , and τ were determined to give reasonable values of compressibility, saturation density, and a binding energy. The density distribution of the i th nucleon is defined by

$$\rho_i(\mathbf{r}) = (2\pi L)^{-2/3} \exp \left[-\frac{(\mathbf{r} - \mathbf{R}_i)^2}{2L} \right], \quad (3)$$

where L represents the width of the Gaussian wave packet of 2.0 fm^2 . Then the overlap density (ρ_i) is given by

$$\begin{aligned} \langle \rho_i \rangle &\equiv \sum_{j \neq i} \rho_{ij} \equiv \sum_{j \neq i} \int d\mathbf{r} \rho_i(\mathbf{r}) \rho_j(\mathbf{r}) \\ &= \sum_{j \neq i} (4\pi L)^{-2/3} \exp \left[-\frac{(\mathbf{R}_i - \mathbf{R}_j)^2}{4L} \right]. \end{aligned} \quad (4)$$

The parameter C_s for the symmetry energy term has been determined to be 25 MeV. The Coulomb potential is given by the error function expressed with "erf," and the parameter c_i representing the number of charge of the i th nucleon; zero for neutron and unity for proton. The elementary charge is given by e .

In addition to the Newtonian equation, two body collisions are taken into consideration for the time evolution of the system. The conventional Cugnon parametrization form [11] was applied to NN scattering cross sections and the angular distribution.

We conducted simulations of more than 3×10^5 proton-nucleus reactions for reasonable statistics. Before each reaction simulation, nuclear ground state was generated using random numbers for nucleon positions and momenta, and checked in terms of the binding energy within 5% to the prediction of the liquid drop model. The b parameter was chosen between zero and $b_{\max} = 1.2A^{1/3} + 5.5 \text{ fm}$. The double differential cross sections were finally determined by normalization in terms of the geometrical cross section equal to πb_{\max}^2 .

In Fig. 3, nucleon densities in the QMD ground state are compared with empirical ones of Negele [19] and de Vries [20]. Thin lines are the distributions of the standard QMD. Since the QMD is based on the classical equation of motion, its ground state is not unique. Therefore, these distributions were made by sampling of nucleon positions from ten thousand of produced nuclei. Dotted and dotted-and-dashed lines show predictions of Negele [19] and de Vries [20], respectively. In the present work, neutrons were assumed to distribute with the same shape as protons and were normalized to give the number of neutrons involved in the nucleus in order to obtain nucleon densities. From a comparison of the radius of the half-maximum of density in Fig. 3, it is found that the QMD distribution is smaller than realistic one by about 25% for ^{12}C and 20% for ^{27}Al . Meanwhile, the difference is relatively smaller for the heavier nucleus ^{93}Nb , and is about 10%.

Momentum distributions are shown in Fig. 4. Dotted lines are results of Hartree-Fock calculations. It is obvious that the standard QMD given by thin lines fails to reproduce the high momentum component for ^{12}C and ^{27}Al . However, a reasonable distribution is obtained for ^{93}Nb .

From the above reasons, it has been concluded that the QMD ground state needed to be modified for larger radii and momenta. However, it is difficult to generate such a bound system in the framework of molecular dynamics. We, therefore decided to change the Skyrme potentials of Eq. (2). For ^{12}C , values of two parameters C_A and C_B were increased to obtain a higher attractive force. We searched the optimum set of C_A and C_B that allows realistic distributions as well as long-time

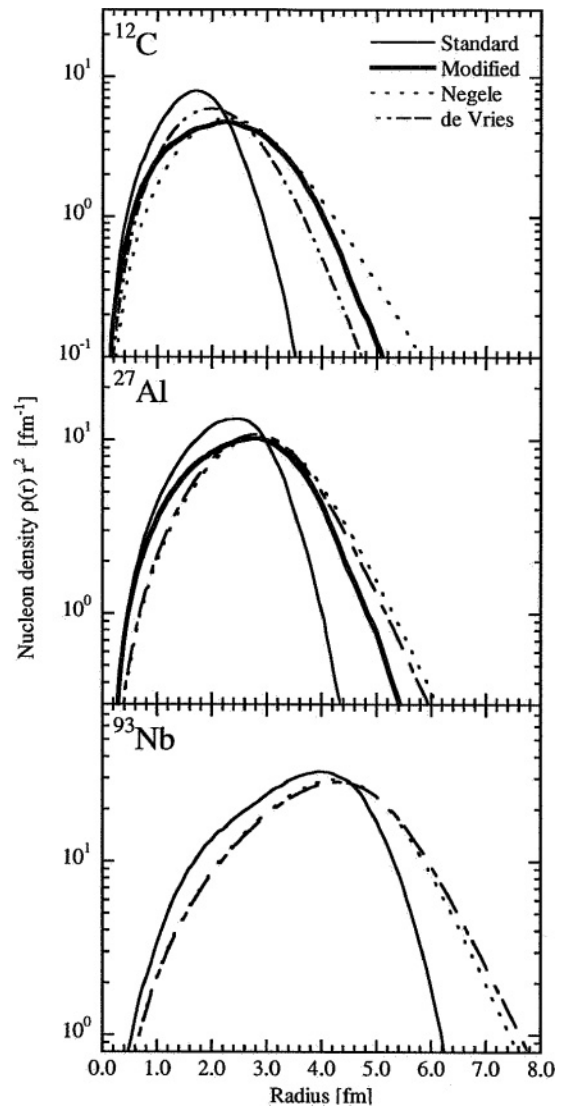


FIG. 3. Nucleon density distributions of ^{12}C , ^{27}Al , and ^{93}Nb . Thin and thick lines are density distribution of the standard, and the modified ground state in the QMD, respectively. Parametrization of Negele [19] and de Vries [20] are also shown.

stability up to 300 fm/c and reasonable binding energy within 5% to a prediction of the standard liquid drop model. For ^{27}Al , the parameter C_s of the symmetry energy term had to be increased in addition to C_A and C_B .

The best parameter sets are listed in Table I. Results of the modified QMD which uses the new parameters are shown by thick lines in Figs. 3 and 4 for ^{12}C and ^{27}Al . It is found that distributions have been improved and are in agreements with Hartree-Fock predictions except for ^{12}C . In order to discuss the inconsistency for ^{12}C , the Hartree-Fock calculation is compared with a relativistic theory [21]. The momentum distribution for ^{16}O is shown in Fig. 5. Although the result of the modified QMD is smaller than the Hartree-Fock calculation, it is consistent with the relativistic theory. This fact may imply that the result for ^{12}C is allowable. In the present work, density and momentum distributions are essential, and

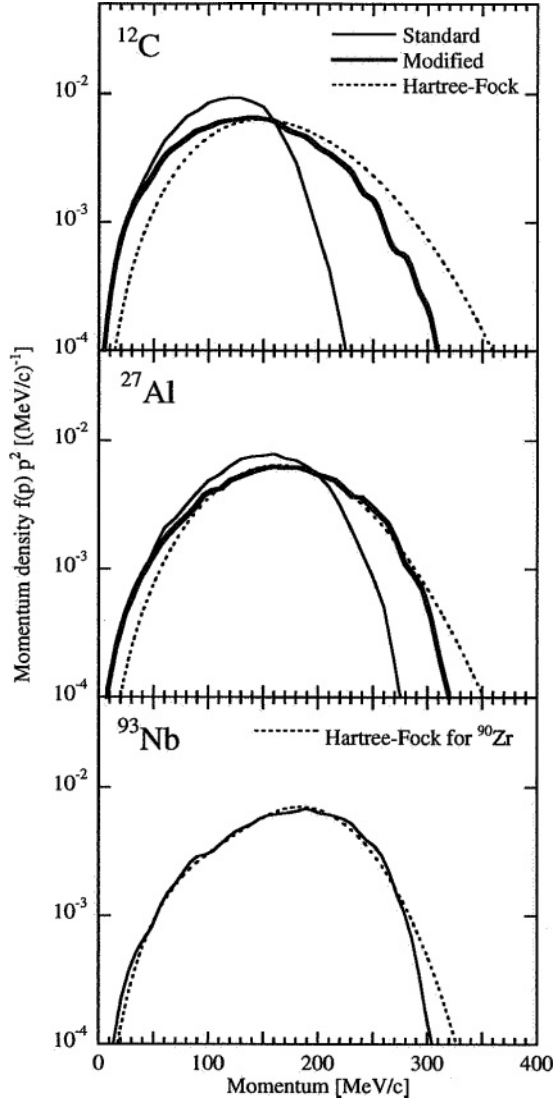


FIG. 4. Momentum density distributions of ^{12}C , ^{27}Al , and ^{93}Nb . Thin and thick lines are momentum distribution of the standard and the modified ground state in the QMD, respectively. The dotted lines show solutions of the Hartree-Fock equations [22].

other quantities such as curvature and compressibility are out of the scope. Therefore, we did not check these quantities.

As for the ^{93}Nb , a ground state having reasonable distributions is generated with the modified QMD. However, the nucleus is unstable and disintegrates in a very short duration time. As discussed above, the ^{93}Nb nucleus produced by the

TABLE I. Parameters used for modifying the QMD.

Target	C_A (MeV)	C_B (MeV)	C_s (MeV)
default	-219.4	165.3	25.0
^{12}C	-394.4	297.5	25.0
^{16}O	-394.4	297.5	25.0
^{27}Al	-394.4	297.5	45.0

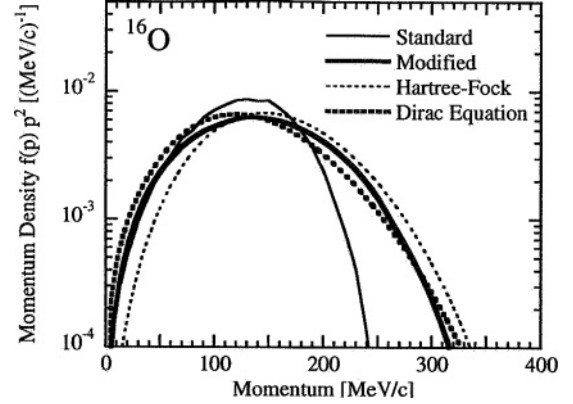


FIG. 5. Momentum density distributions for ^{16}O . The thin and the thick lines are results of the standard and the modified QMD, respectively. They are compared with the Hartree-Fock (the thin dotted line) and the relativistic mean field (the thick dotted line) calculations.

original QMD is not very bad. We decided to use the original one, since they are stable enough.

B. Intranuclear cascade model

The INC model is widely known to be a powerful tool to simulate a variety of nuclear reactions in an intermediate energy range. Although there are several codes, which are open for use, they are not suitable to investigate the reaction mechanism in detail. We have considered that a good description of the target ground state is necessary for high reproducibility of reactions in the energy range 300 to 400 MeV. Therefore, we have coded a program originally in order to prove the importance of the ground state.

In the phase of generating ground state, nucleons are distributed in r and p spaces independently. Initial nucleon positions were determined stochastically by using a weighting function to simulate the Woods-Saxon type density distributions:

$$f_{ws}(r) = \frac{1}{1 + \exp[(r - R_{\text{nucl}})/a]}, \quad (5)$$

with

$$R_{\text{nucl}} = 1.20 \times A^{1/3},$$

where a is the diffuseness parameter and A the mass number. We used a value of 0.5 for a . And the maximum nuclear radius was chosen to be $R_{\text{nucl}} + 5.5$ fm. In addition, each nucleon is prohibited to be close to other nucleons within 1.5 fm in r space to simulate the Pauli exclusion principle in the ground state. Inside the nucleus, each nucleon is assumed to feel a uniform potential of -42 MeV. The Fermi momentum of each nucleon was chosen randomly to reproduce distributions of the modified QMD for ^{12}C and ^{27}Al . For ^{93}Nb , distributions of the standard QMD were referred.

In the reaction phase, the nucleons are classified into two groups: one is a participant and another spectator. The spectator nucleons have energies below the Fermi surface. The participant is the nucleons in the continuum energy

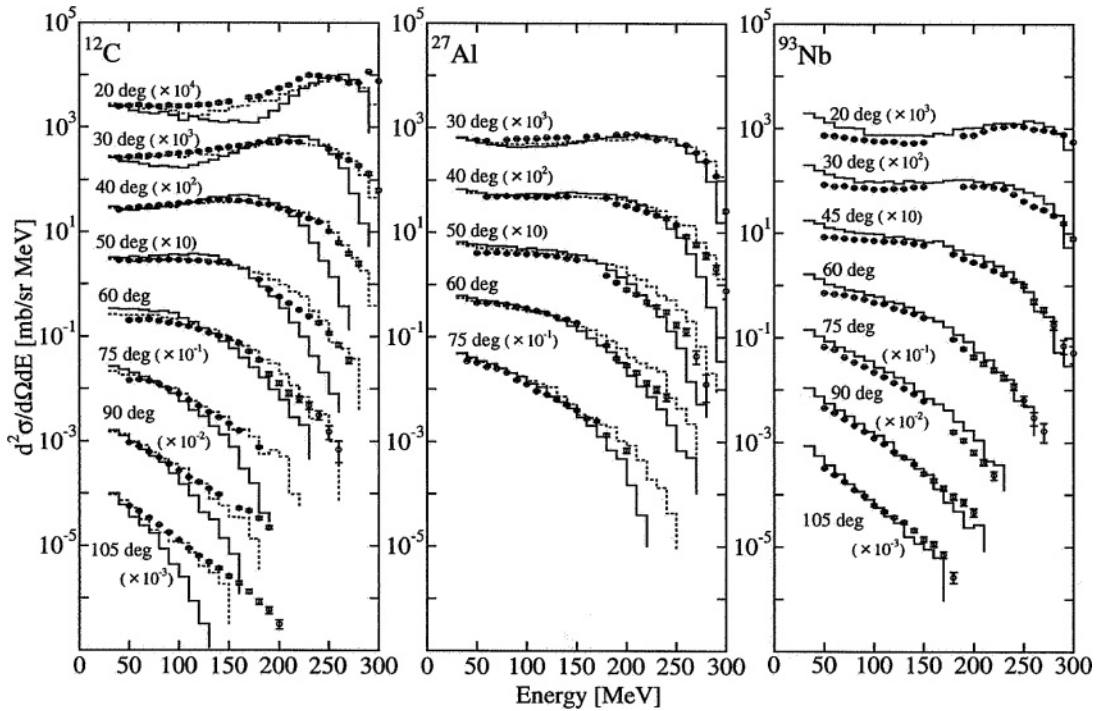


FIG. 6. Spectra of double differential cross section for $(p, p'x)$ at 300 MeV with the standard (solid lines) and modified (dotted lines) QMD.

domain, which can potentially induce nuclear reactions. This prescription is same as that used generally in many INC models, such as the Bertini [6–8] and the ISOBAR [13–15] models. As time evolves, sole participant nucleons are traced to travel along a straight-line trajectory. Since a uniform nuclear potential is assumed, their momenta are constant through the time development inside the nucleus. When a participant particle approaches to one of the nucleons closer than a distance determined by two-body scattering cross sections, they will undergo scattering. The Cugnon prescription [11] was used to treat two-body scattering for not only the cross sections but also the Pauli blocking effect. In the present experiment, no data were measured below 40 MeV, we are not concerned with the low energy regime; therefore, the reflection at the potential surface including the Coulomb barrier and the particles evaporation were ignored. The time development was made for 120 fm/c. It is long enough for all of energetic particles leaving the nucleus.

The absolute double differential cross sections were obtained with the same fashion as in the QMD calculations. Normalization was made in terms of the geometrical cross section πb_{max}^2 . To obtain good statistics, nuclear reactions were simulated 5×10^5 times.

V. RESULTS AND DISCUSSION

A. Experimental data

The double differential cross sections obtained in our study have been shown in Figs. 6 and 7 with open circles for $(p, p'x)$ reactions on C, Al, and Nb at 300 and 392 MeV. Energy

distributions have been obtained in a range of 400 MeV down to 40 MeV at seven or eight angles within 20° – 105° . Due to the thickness of the second and third plastic scintillators, cross sections could not be measured for the energy region below 30 MeV. Each data point in the figures represents the double differential cross section for every 10-MeV bin. This bin width is comparable to the energy resolution of the detectors. The error bar at each data point shows statistical error.

Forward angle spectra show clear and broad peaks in all reactions. These are considered to be quasifree peaks. Their peak energies are consistent with that of free proton-nucleon scattering at the corresponding angle. Their width is known to reflect the Fermi motion of nucleons inside nucleus. No other significant structures have been observed. With increasing angles, the strength of quasifree peaks becomes smaller. At last no structure is seen at large angles.

There are some missing data around 160 MeV and 230 MeV. At these energies, proton ranges in GSO are slightly longer than the depth of single and double cubic crystals, respectively. Protons that barely pass borders of scintillators would produce pulses of small amplitudes. Such signals are interfered by indistinguishable pulses due to PMT noise or γ -ray background. As a result, some spectra include structures enhanced unexpectedly due to the interference. Such abnormal data points have been deleted in the present work. The last two experimental points for ^{12}C at 20° induced by 300 MeV protons are the peak of elastic scattering. The second point from the last for ^{12}C at 20° induced by 392 MeV protons is same. Both of their cross sections are about 10 mb/sr. The values are reasonable compared with Ref. [23].

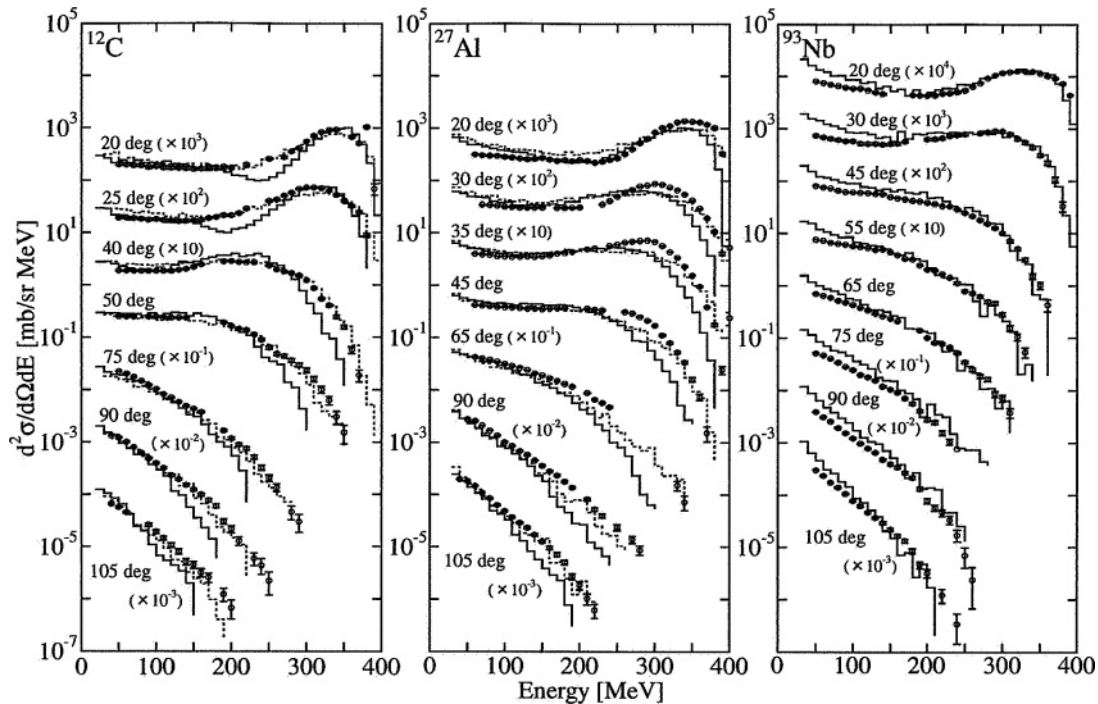


FIG. 7. Same as Fig. 6, but for reactions at 392 MeV.

B. Comparison with QMD

In Figs. 6 and 7, QMD results have been compared with measured data. Solid and dotted lines present QMD results with the standard and the modified ground states, respectively. In the measured spectra for ^{12}C , quasifree peaks are clearly observed at forward angles. At the higher energy side of the peak of spectrum at 20° , the QMD gives reasonable account to the measured data. However, at the lower energy side, large discrepancy is observed. The measured data decreases gradually with decreasing energy but on the contrary, the spectrum of the QMD decreases too rapidly. Moreover, considerable underestimations are observed in the highest energy part of spectra at every angles except for 20° . As shown by dotted lines, the modification of the ground state has succeeded in improving the consistency of the QMD results. The similar tendencies are seen in the case of 392 MeV. The data are well reproduced by the QMD using the modified ground state.

The results for ^{27}Al appear to be similar to that for ^{12}C . At 300 MeV, the QMD calculations are in good agreement with the data. With the modified ground state, better agreements are achieved at 30° and 40° . However, the modified one gives overestimations at 50° and 60° instead of underestimation with the standard one. At 392 MeV, consistency becomes relatively better at all angles. Discrepancies are still prominent in the higher energy part of the spectra.

In the measured spectra for ^{93}Nb , quasifree peaks are not very clear. The QMD gives good overall account to the data of 300 MeV, except for slight overestimations in the lowest energy part. At 392 MeV, the discrepancies in the lowest energy region become larger. Such overestimations show tendency to increase with decreasing the outgoing proton energy.

C. Comparison with INC

Figures 8 and 9 show the energy distributions of protons, as in Figs. 6 and 7, respectively, for INC models. Broken lines indicate results of the Bertini code [6–8] which is one of the most popular INC codes used in the intermediate energy domain. This code is used for an intranuclear reaction part of the PHITS [24] code, and the double differential cross section values have been normalized by using total reaction cross sections in the present work. The results of the Bertini model are in poor agreement with the experimental data. Especially for ^{12}C , there are noticeable discrepancies at all angles and the both incident energies. At 300 MeV, the quasifree peaks appear to be too prominent due to underestimation for the lower energy domain of the peak region. At large angles from 40° to 105° , the calculations decrease too rapidly with increasing outgoing proton energy and thus there is significant underestimation for the higher energy part of spectra. Although at 392 MeV there are large discrepancies and the tendency is similar to that in the case of 300 MeV, better accounts have been obtained. The effect of the Fermi momenta can be expected to be less important with increasing incident energy. Results for ^{27}Al are similar to those of ^{12}C . However, slightly better agreements have been obtained at 20° of 392 MeV. For ^{93}Nb , further better agreements are shown. From the above discussion, a conclusion can be drawn that the Bertini model has a tendency to give better account to data with increasing mass number of target nuclei and bombarding particle energy.

Results of the present INC model are displayed by the solid lines in Figs. 8 and 9. It is demonstrated that fairly good agreements have been achieved with the present INC. In comparison with the results of the QMD, the present INC

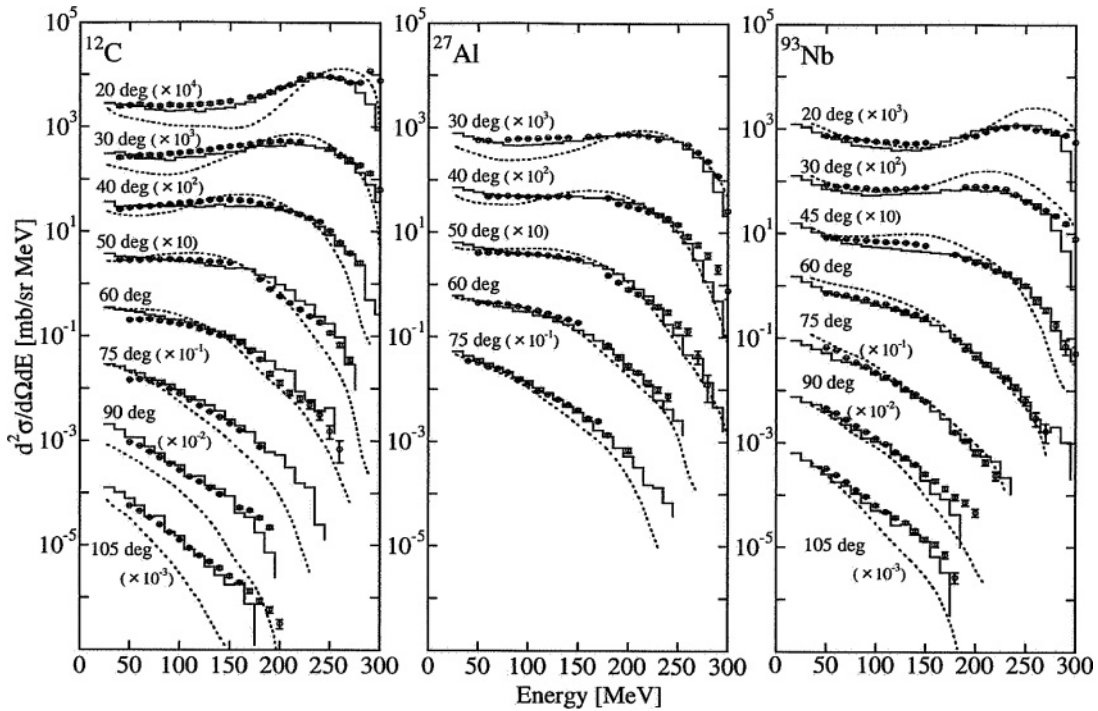


FIG. 8. Spectra of double differential cross section for $(p, p'x)$ at 300 MeV with the present INC (solid lines) and the Bertini (dotted lines).

calculation appears to have the higher predictive ability. It should be reminded that the modified QMD show discrepancies for the 20° data of ^{12}C 300 MeV and ^{27}Al 392 MeV, they are accounted with the present INC model satisfactorily. Moreover, the QMD overestimates the low energy part of the

spectra for ^{93}Nb ; the INC, on the other hand, shows fairly good consistencies.

The differences in results between the three calculations such as the present INC, the Bertini code, and the QMD are ascribed mainly to the ground state of target nuclei used in

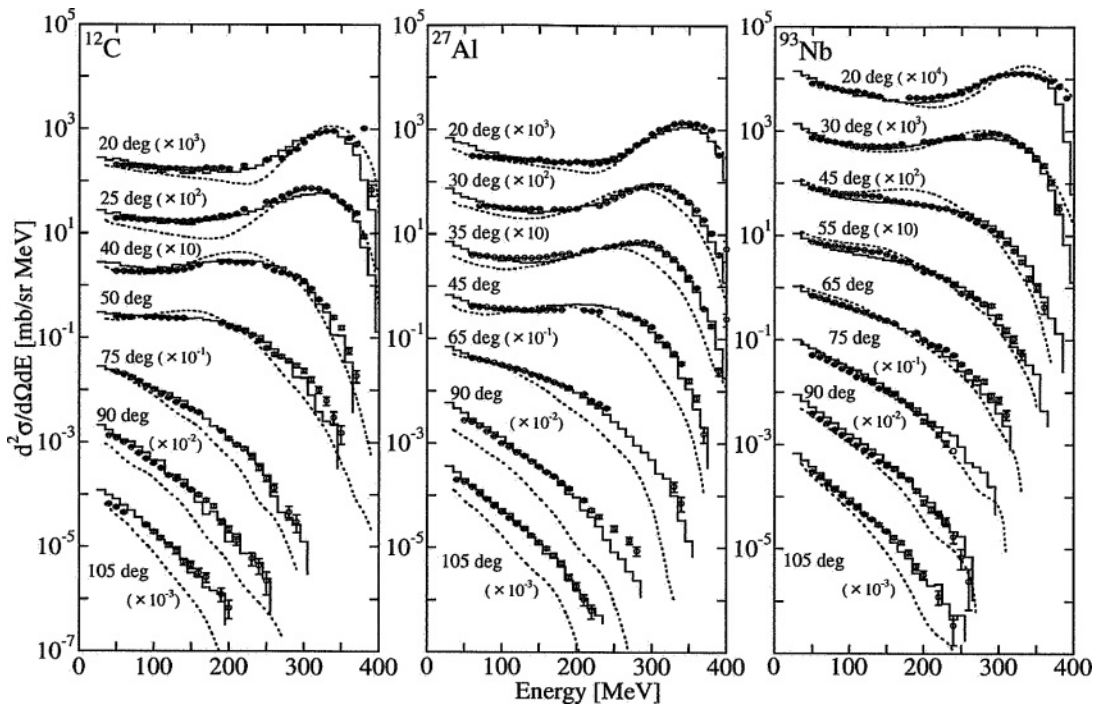


FIG. 9. Same as Fig. 8, but for reactions at 392 MeV.

calculations because all of them use the same NN cross sections. The most realistic ground states are applied to the present INC calculations. However, the Bertini treats nuclear ground state roughly; the radial variation of the nuclear density is taken into account by dividing the nucleus into eight concentric zones of different constant density. And the momentum distribution is treated by the local density approximation. In particular, it is known that a step function approximation is poor to describe nuclear density distribution of light nucleus such as ^{12}C and ^{27}Al . The resultant energy distributions of Bertini, therefore, reveal rather large discrepancies for the two nuclei. In the case of the QMD, it is difficult to realize the realistic ground state. As discussed above, the generated distributions are different from the measured one even in the modified version.

VI. CONCLUSION

Experiments for double differential cross sections of $(p, p'x)$ reactions have been conducted to facilitate compiling new nuclear data libraries for applications. Energy spectra have been measured on ^{12}C , ^{27}Al , and ^{93}Nb at incident energies of 300 and 392 MeV. The results have been compared with the

INC and the QMD model calculations to check the reliability of these calculations. Several conclusions have been drawn from comparison of the experimental results with theoretical calculations. First, the INC model can give overall good account to the data by employing realistic ground states for target nuclei. However, the currently available version of the INC Bertini code shows rather large discrepancies. Secondly, the QMD calculation can be improved remarkably by modification of ground state distributions; however, noticeable disagreements are seen in the lower energy part of the spectra of the heaviest target Nb at the incident energy of 392 MeV. Thirdly, usage of realistic ground state distribution is essential in the INC and the QMD models for high predictive ability of the intermediate energy $(p, p'x)$ reactions.

ACKNOWLEDGMENTS

The authors would like to thank Professor Hatanaka and the RCNP cyclotron crews for their assistance in this research. This research was partly supported by the Grant-in-Aid for Scientific Research, Ministry of Education, Science, Culture and Sports, Grant No. 13480149.

-
- [1] W. N. Hess and B. J. Moyer, *Phys. Rev.* **101**, 337 (1956).
 - [2] J. W. Wachter, W. A. Gibson, and W. R. Burrus, *Phys. Rev. C* **6**, 1496 (1972).
 - [3] A. A. Cowley, G. F. Steyn, Y. Watanabe, T. Noro, K. Tamura, M. Kawabata, K. Hatanaka, H. Sakaguchi, H. Takeda, and M. Itho, *Phys. Rev. C* **62**, 064604 (2000).
 - [4] J. Aichelin, *Phys. Rep.* **202**, 233 (1991).
 - [5] K. Niita, S. Chiba, T. Maruyama, H. Takada, T. Fukahori, Y. Nakahara, and A. Iwamoto, *Phys. Rev. C* **52**, 2620 (1995).
 - [6] H. W. Bertini, *Phys. Rev.* **131**, 1801 (1963).
 - [7] H. W. Bertini, *Phys. Rev.* **188**, 1711 (1969).
 - [8] H. W. Bertini, *Phys. Rev. C* **6**, 660 (1972).
 - [9] Y. Yariv and Z. Fraenkel, *Phys. Rev. C* **20**, 2227 (1979).
 - [10] G. D. Harp, K. Chen, G. Friedlander, Z. Fraenkel, and M. Miller, *Phys. Rev. C* **8**, 581 (1973).
 - [11] J. Cugnon, *Phys. Rev. C* **22**, 1885 (1980).
 - [12] A. Boudard, J. Cugnon, S. Leray, and C. Volant, *Phys. Rev. C* **66**, 044615 (2002).
 - [13] R. M. Sternheimer and S. J. Lindenbaum, *Phys. Rev.* **105**, 1874 (1957).
 - [14] R. M. Sternheimer and S. J. Lindenbaum, *Phys. Rev.* **109**, 1723 (1958).
 - [15] R. M. Sternheimer and S. J. Lindenbaum, *Phys. Rev.* **123**, 333 (1961).
 - [16] K. Anami *et al.*, *Nucl. Instrum. Methods Phys. Res. A* **404**, 327 (1998).
 - [17] H. Yoshida *et al.*, *Nucl. Instrum. Methods Phys. Res. A* **411**, 46 (1998).
 - [18] M. Makino, R. Eisberg, D. Ingham, and C. Waddell, *Nucl. Instrum. Meth.* **81**, 125 (1970).
 - [19] J. W. Negele, *Phys. Rev. C* **1**, 1260 (1970).
 - [20] H. de Vries, C. W. de Jager, and C. de Vries, *At. Data Nucl. Data Tables* **36**, 495 (1987).
 - [21] M. Nakano (private communication).
 - [22] M. Sandel and J. P. Vary, *Phys. Rev. C* **20**, 744 (1979).
 - [23] R. E. Richardson, W. P. Ball, C. E. L., Jr., and B. J. Moyer, *Phys. Rev.* **86**, 29 (1952).
 - [24] H. Iwase, K. Niita, and T. Nakamura, *J. Nucl. Sci. Tech.* **39**, 1142 (2002).